

INFLUENCE OF ZIRCONIUM ON THE CRYSTALLIZATION OF ETS-10 MOLECULAR SIEVE

D. Vuono^{1*}, C. C. Pavel², P. De Luca¹, J. B. Nagy³ and A. Nastro¹

¹Dipartimento di Pianificazione Territoriale, University of Calabria, via P. Bucci, C.A.P. 87036, Arcavacata di Rende (CS), Italy

²Department of Chemical Technology and Materials Chemistry, Faculty of Chemistry, ‘Al. I. Cuza’ University of Iasi, Bd. Carol I, 6600 Iasi, Romania

³Laboratoire de R.M.N., Facultés Universitaires Notre-Dame de la Paix, 5000 Namur, Belgium

The ETS-10 is a newly formed titano-silicate the structure of which was resolved thanks to the XRD, EDS, HREM and mass NMR. The ETS-10 is a potentially good catalyst. The aim of this research is to study the physicochemical properties of ET(Zr)S-10 obtained from a gel containing different amounts of Zr. The analyses used are XRD, thermal analysis (TG-DSC), SEM, and ²⁹Si NMR.

Keywords: DSC, ETS-10, initial gels, TG, zirconium

Introduction

In 1989 Kuznicki synthesized new titanium based materials [1]. Chapman in 1990 synthesised microporous titanosilicate used as molecular sieves [2]. The ETS-10 is a newly formed titano-silicate the structure of which was resolved thanks to the XRD, EDS, HREM and mass NMR [3]. The structure contains TiO₆ octahedra, two oxygen atoms being shared by neighboring TiO₆ units forming a Ti–O–Ti chain, while the other four oxygen atoms are shared with neighboring tetrahedral SiO₄ groups [3, 4]. A set of periodically placed chains develops that way in an orthogonal direction. The superimposition of layer of this type gives rise to a tridimensional structure of 12 membered ring channels. Only few zeolitic structures have such an open structure, the more important ones being zeolite Y (FAU) and zeolite Beta (BEA). Each titanium atom in this structure is associated with two negative charges that are neutralized by cations not being part of the structure. The density of cations is roughly similar to that of a zeolite with Si/Al=2.5. Due to the long interconnecting pores in the structure and the high density of the extraframework cations, the ETS-10 is a potentially good catalyst. In addition, aluminium can be substituted at tetrahedral positions replacing silicon and hence Broensted acid sites can be introduced [5, 6]. In ETS-10, the disposition of the layers composed of Ti–O–Ti chains in an orthogonal way is not regular leading to defects in the structure. The disorder can be modelled by the combination of two polymorphic structures that are due to different sequences. The polymorph A corresponds to a sequence ABCD and has a monoclinic symmetry with C2/c space

group, while the other corresponds to a sequence ABAB and has a tetragonal symmetry with space group P41 or P43 [7]. Eldewik *et al.* have investigated the incorporation of Co²⁺ ions into ETS-10 [8]. Neither the physicochemical nor the catalytic properties of ETS-10 are well characterized. Anyway it is not clear how they could be influenced by the disorder. Anderson *et al.* used a combination of atomic force microscopy, high-resolution electron microscopy and modelling to elucidate the details of the mechanism of crystal growth in framework of ETS-10 and other materials [9]. Kim *et al.* reported studies on the crystallization of ETS-10 using various compositional systems in presence of organics and in the absence of seeds [10, 11]. Picquart *et al.* studied the chemical-physical behaviour of sol-gel zirconia [12]. Naik *et al.* synthesized a sodium zirconium phosphate, potential ceramic matrix for fixation of high level nuclear waste [13].

Experimental

The synthesis procedure for ETS-10 molecular sieves is identical to that proposed by Pavel *et al.* [14]. Two batches are separately prepared, the one being alkaline and the other acidic. For the alkaline batch the ingredients are added in the following order: sodium silicate (Merck; 8% Na₂O, 27% SiO₂, 65% H₂O), sodium hydroxide (Carlo Erba; 50 mass%) and potassium fluoride (Merck; 40 mass%). For acidic batch the components are added in the following order: distilled water, hydrochloric acid (Carlo Erba; 37 mass%), titanium tetrachloride (Merck; 50 mass%) and zirconium tetrachloride in

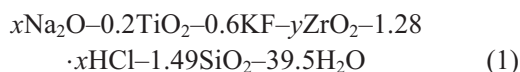
* Author for correspondence: danyvuono@yahoo.it

powder (Acros; purity 98%). After a short homogenization of both batches the solutions are stirred during 10 min, the acidic batch is poured into the alkaline one producing a gel. The gels are introduced into PTFE-lined Morey type inox steel autoclaves of 50 cm³. The temperature of reaction was 190°C in thermoventilated oven in static conditions.

The XR diffractograms are registered on a Philips PW 1830 diffractometer using CuK_α radiation. The velocity was 0.02° s⁻¹ in the range of 5–45° 2θ. The thermal analysis was carried out on a Netzsch 429 instrument. The temperature range was 20–750°C with a velocity of heating of 10 K min⁻¹ in static air. The pH of gels and the mother liquors were determined by Crison GLP 22 pH-meter. The ratios Si/Ti and Si/Zr were determined by EDS ZAF-4/FLS. The morphology of the crystals is studied by SEM Stereoscan 360S scanning electron microscope. Magic Angle Spinning ²⁹Si NMR spectra were taken on a Bruker MSL 400 spectrometer at 79.4 MHz. A 4.0 μs pulse ($\theta=\pi/4$) and a repetition time of 6.0 s were used.

Results and discussion

The following compositions were used (System (1))



with $0.5 \leq x \leq 1.2$ and $0.0 \leq y \leq 0.2$. The crystallization fields to obtain a pure ET(Zr)S-10 phase is quite small with respect to those of ET(Zr)S-4. Indeed, the formation of ET(Zr)S-10 is more difficult and requires a relatively low ZrO₂ (maximum 0.06 moles) and a medium alkalinity $0.85 \leq \text{Na}_2\text{O} \leq 1.15$. Table 1 shows the Si/Ti and Si/Zr values for the initial and intermediate phases for the synthesis of ET(Zr)S-10 with 0.03 moles of ZrO₂. The first crystalline phase shows a higher Si/Ti ratio and a higher Si/Ti ratio than the initial amorphous phase. Later on the Si/Ti ratio slightly decreases and it is close to 4 for the final crystalline sample. The Si/Zr ratio increases continuously during the crystallization. However, the Zr content remains low in individual crystals showing the difficulty to introduce Zr in the structure. The morphology of the crystals does not change as a function of time (Fig. 1), but the presence of an amorphous phase can be noted at intermediate times of crystallization. The form of the crystals is a parallelepiped with a quadratic basis. If the amount of ZrO₂ increases in the initial gel, the Si/Ti ratio decreases from 4 to 3.7 (Table 2), and the Si/Zr ratio also decreases showing that more Ti and more Zr are introduced in the ET(Zr)S-10 samples. The thermal analysis of the intermediate phases also led to interesting conclusions. Figure 2 shows the TG (Fig. 2a), DTG (Fig. 2b) and DSC (Fig. 2c) curves of the ET(Zr)S-10 sample syn-

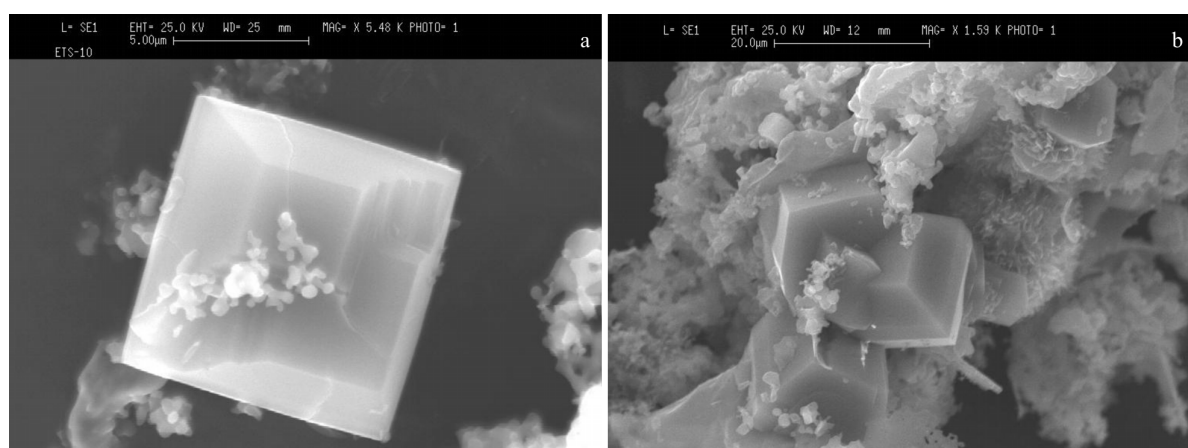


Fig. 1 SEM of the solid products obtained from the reacting system:
 $1.0\text{Na}_2\text{O}-0.2\text{TiO}_2-0.6\text{KF}-y\text{ZrO}_2-1.28\text{HCl}-1.49\text{SiO}_2-39.5\text{H}_2\text{O}$; a – Y=0.03, b – Y=0.06. Reaction time: 36 h

Table 1 Si/Ti and Si/Zr ratio vs. crystallization time for system:
 $1.0\text{Na}_2\text{O}-0.2\text{TiO}_2-0.6\text{KF}-0.03\text{ZrO}_2-1.28\text{HCl}-1.49\text{SiO}_2-39.5\text{H}_2\text{O}$

Crystallization time/h	Si/Ti	Si/Zr
12 (amorphous)	2.6	29
18	4.7	70
24	4.2	117
36	4.2	133
76	4.1	140

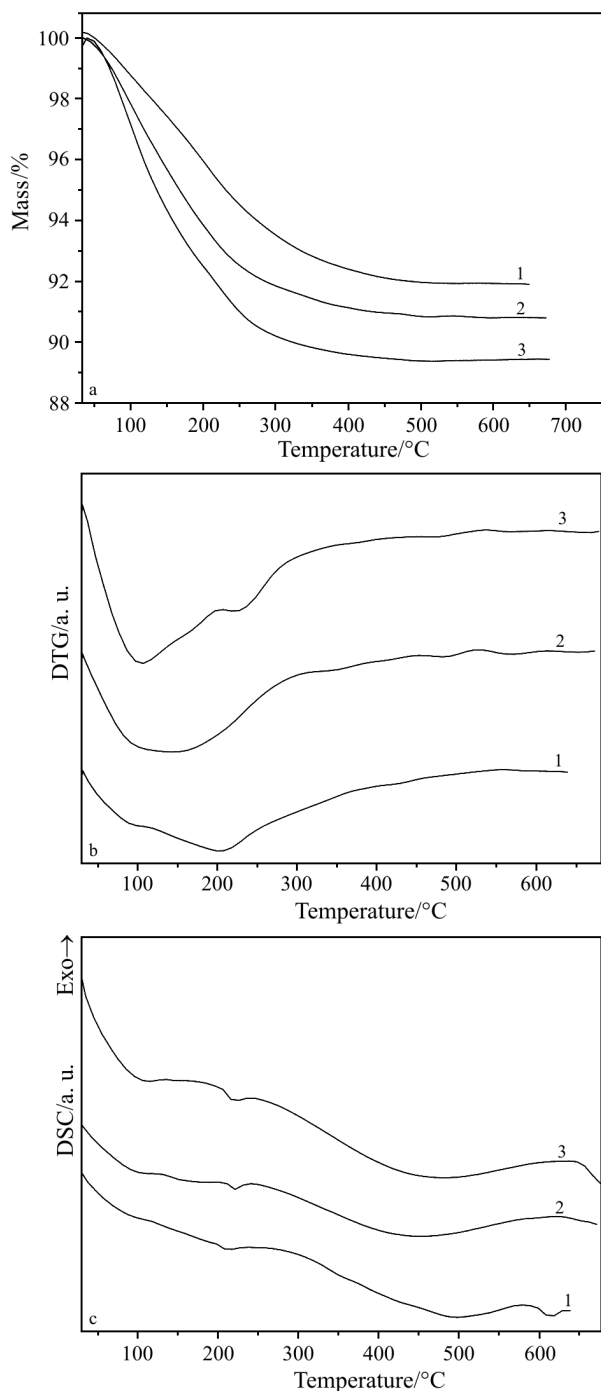


Fig. 2 a – TG, b – DTG and c – DSC curves for three different ET(Zr)S-10 synthesized with $1.0\text{Na}_2\text{O}$ and 0.03ZrO_2 samples: 1 – initial gel, 2 – ET(Zr)S-10 at 50% crystallinity, 3 – ET(Zr)S-10 at 85% crystallinity

thesized with $1.0\text{Na}_2\text{O}$ and 0.03ZrO_2 in the initial gel. The mass losses are due to the desorption of water at ca. 100 and at 220°C (Table 3). The mass loss in peak I increases during crystallization, while that of peak II decreases. The total mass loss increases due to the increase in peak I. The correct attribution of the

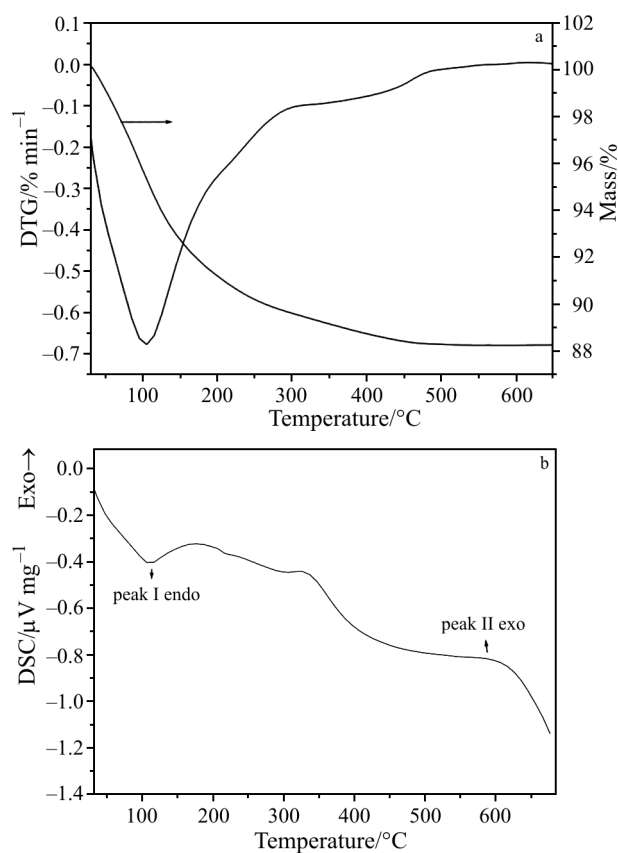


Fig. 3 a – TG and DTG curves of sonicated ET(Zr)S-10 85% crystalline sample, b – corresponding DSC curves

various peaks can be made comparing these results with those of a sonicated, i.e. pure crystalline ET(Zr)S-10 sample. The results for the latter are illustrated in Fig. 3 and the data are reported in Tables 3 and 4. It is clearly seen that the second peak at 220°C is absent in the pure crystalline sample. The explanation of the two peaks is hence the following. The first peak at ca. 110°C is essentially due to the desorption of zeolitic water. Its amount increases during crystallization showing the more porous nature of the crystalline phase. The second peak is due to the loss of water from the amorphous phase. Indeed, it is absent in the pure crystalline phase and its amount decreases with increasing crystallization time. The third peak at ca. 620°C not accompanied by any mass loss is quite different for the amorphous gel phase at one hand and for the crystalline ET(Zr)S-10 phases at the other hand. Indeed, this peak is endothermal for the gel phase, it is due to the fusion of the material yielding a vitrorous phase formed by droplet-like balls, that are characteristic of vitrification of the material after a fast cooling. This peak is exothermal for samples containing the crystalline ET(Zr)S-10 phase. This corresponds to the transformation of an open ETS-10 struc-

Table 2 Si/Ti and Si/Zr ratios *vs.* crystallization time for system:
1.0Na₂O–0.2TiO₂–0.6KF–0.06ZrO₂–1.28HCl–1.49SiO₂–39.5H₂O

Crystallization time/h	Si/Ti	Si/Zr
18 (amorphous)	4.0	16.1
24	4.4	170
36	4.2	130
76	3.7	99
100	3.7	99

Table 3 Mass losses of various ET(Zr)S-10 samples

Sample	Peak I/%	Peak II/%	Total mass loss/%
amorphous	1.62	6.27	7.89
ET(Zr)S-10 50%	4.20	3.85	8.05
ET(Zr)S-10 85%	7.16	2.82	9.98
sonicated ET(Zr)S-10	11.75	—	11.75

Table 4 Temperature of the maxima of DSC curves of various ET(Zr)S-10 samples

Phase/%	T _{max} peak I endo/°C	T _{max} peak II endo/°C	T _{max} peak III exo/°C
amorphous	91.0	213.2	614.7 (endo)
ET(Zr)S-10 50%	106.1	220.8	621.7
ET(Zr)S-10 85%	114.4	221.4	639.9
sonicated ET(Zr)S-10	109.8	—	620.1

Table 5 Chemical composition of ETS-10 and ET(Zr)S-10 samples synthesized at 190°C from an initial gel of composition:
1.0Na₂O–0.2TiO₂–0.6KF–1.28HCl–YZrO₂–1.49SiO₂–39.5H₂O

Sample	Y	Na _{u.c.} /moles	K _{u.c.} /moles	Na+K _{u.c.}	Ti _{u.c.} /moles	Zr _{u.c.} /moles
ETS-10	0.0	1.58	0.42	2.00	1.00	—
sonicated ET(Zr)S-10	0.03	1.33	0.53	1.86	0.92	0.08

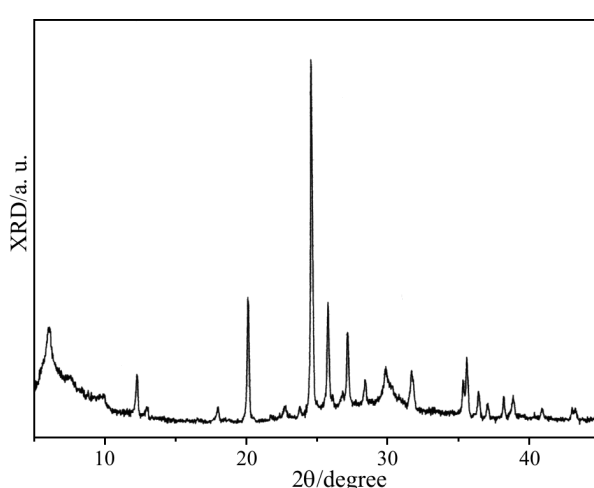


Fig. 4 XRD spectra of the sonicated ET(Zr)S-10 obtained with 1.0Na₂O and 0.03TiO₂

ture to dense titanosilicate phases. The chemical analysis data are compared for a pure ETS-10 sample and a pure ET(Zr)S-10 sample both obtained with 1.0Na₂O and 0.03ZrO₂ (Table 5). The Ti content decreases together with the Na and K content. It is suggested, because the (Ti+Zr) content remains constant that Zr is replacing Ti in the structure. Figure 4 shows the XR diffractogram of the sonicated ET(Zr)S-10 sample. The *d*-spacing values are reported in Table 6. Figure 5b shows high power proton decoupled ²⁹Si NMR spectra of the intermediate and final ET(Zr)S-10 phases while Table 7 reports the relative silicon amount in the samples. The NMR lines of the ETS-10 phase are easily recognised. Indeed, the lines at -94.8 and -96.8 ppm stem from the Si(3Si,1Ti) configurations, while the -104.2 ppm line stem from Si(4Si,0Ti) configuration [3]. Note that the relative intensities of these NMR lines are close to 2:2:1

Table 6 *d*-spacing values for ETS-10 and ET(Zr)S-10 samples

ETS-10		ET(Zr)S-10	
20	<i>d</i> -value	20	<i>d</i> -value
6.100	14.4770	6.270	14.0848
9.695	9.1153	10.140	8.7163
12.435	7.1123	12.415	7.1237
13.115	6.7450	13.095	6.7553
18.130	4.8890	18.090	4.8997
20.275	4.3763	20.290	4.3731
23.935	3.7148	23.935	3.7148
24.825	3.5836	24.805	3.5864
25.960	3.4294	25.950	3.4307
27.320	3.2611	27.290	3.2652
28.540	3.1250	28.490	3.1303
30.050	2.9713	29.975	2.9786
31.935	2.8001	31.925	2.8009
35.750	2.5095	35.465	2.5290
36.560	2.4558	35.730	2.5109
37.180	2.4162	36.545	2.4567
38.320	2.3466	37.130	2.4194
41.030	2.1980	40.925	2.2034
43.175	2.0936	43.135	2.0954

which are the theoretical values. The contribution of the amorphous phase at -89 and -98 ppm decreases with increasing crystallisation time. It could be proposed that the ^{29}Si NMR spectra could also be used to follow the crystallisation of the ETS-10 phases as it was previously made for example in the MFI formation [15]. The CP- ^{29}Si NMR spectra yields complementary information (Fig. 5a). Indeed, because the amorphous phase contains many silanol groups and other non-zeolitic silicon species, it dominates the spectra at 24 and 48 h (Figs 5a – 1 and 2). In addition, at 72 and 118 h (Figs 5a – 3 and 4) the various contributions are more differentiated and lines at -80, -85, -90 and -100 ppm are also detected.

Table 7 Intensities of the high power proton decoupled ^{29}Si NMR spectra of ET(Zr)S-10 intermediate and final crystalline phases obtained from the system: 1.0Na₂O–0.2TiO₂–0.6KF–1.28HCl–YzrO₂–1.49SiO₂–39.5H₂O

Crystallization time/h	ET(Zr)S-10				Amorphous	
	Cryst./%	δ/ppm			δ/ppm	
		-94.8	-96.8	-104.2	-89	-87
24	15	14	16	7	17	46
48	60	27	30	15	18	10
72	80	34	36	19	11	–
118	100	35	41	20	4	–

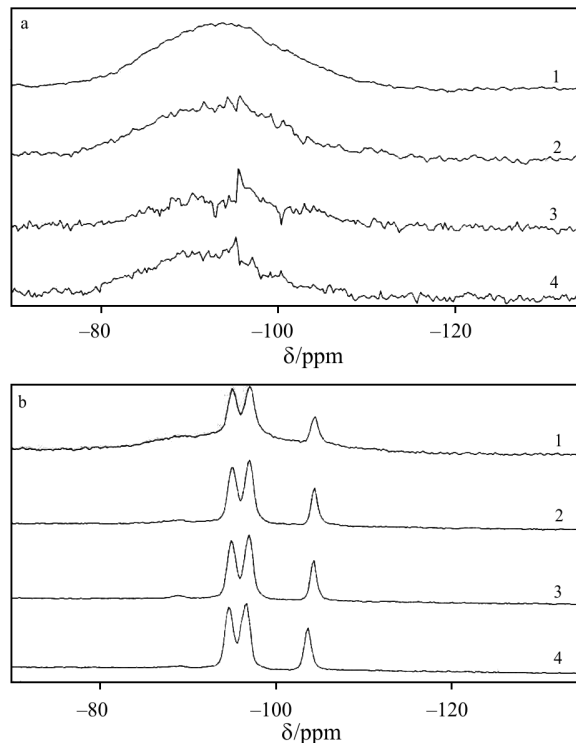


Fig. 5 a – Cross polarised and b – high power proton decoupled ^{29}Si NMR spectra of intermediate and final ET(Zr)S-10 phases obtained from System (1) at 190°C: 1 – 24 h, 2 – 48 h, 3 – 72 h and 4 – 118 h

Conclusions

Zirconium can be easily introduced into the ETS-10 structure using the normal synthesis of ETS-10 by adding both TiCl₄ and ZrCl₄ reagents at the same time to the initial mixture. Up to 0.08Zr_{u.c.} could be introduced in a highly crystalline material.

References

- 1 S. M. Kuznicki, US Patent 4,853202, assigned to Engelhard Corporation, 1989.
- 2 D. M. Chapman, US Patent 5015453, assigned to W. R. Grace and Co.-Conn., 1990.
- 3 M. W. Anderson, O. Terasaki, T. Ohsuna, A. Philippou, S. P. Mackay, A. Ferreira, J. Rocha and S. Lidin, *Nature*, 367 (1994) 347.
- 4 J. Rocha and M. W. Anderson, *Eur. J. Inorg.*, (2000) 801.
- 5 Z. Lin, J. Rocha, A. Ferreira and M. W. Anderson, *Colloids Surf. A*, 179 (2001) 133.
- 6 A. Liepold, K. Roos, W. Reschetilowski, Z. Lin, J. Rocha, A. Philippou and M. W. Anderson, *Microporous Mater.*, 10 (1997) 211.
- 7 X. Yang, J. L. Pallaud, H. F. W. J. Van Breukelen, H. Kessler and E. Duprey, *Microporous Mesoporous Mater.*, 46 (2001) 1.
- 8 A. Eldewik and R. Howe, *Microporous Mesoporous Mater.*, 48 (2001) 65.
- 9 M. W. Anderson, J. R. Agger, N. Hanif and O. Terasaki, *Microporous Mesoporous Mater.*, 48 (2001) 1.
- 10 W. J. Kim, M. C. Lee, J. C. Yoo and D. T. Hayhurst, *Microporous Mesoporous Mater.*, 41 (2000) 79.
- 11 W. J. Kim, S. D. Kim, H. S. Jung and D. T. Hayhurst, *Microporous Mesoporous Mater.*, 56 (2002) 89.
- 12 M. Picquart, T. López, R. Gómez, E. Torres, A. Moreno and J. Garcia, *J. Therm. Anal. Cal.*, 76 (2004) 755.
- 13 A. H. Naik, N. V. Thakkar, S. R. Dharwadkar, K. D. Singh Mudher and V. Venugopal, *J. Therm. Anal. Cal.*, 78 (2004) 707.
- 14 C. C. Pavel, D. Vuono, L. Catanzaro, P. De Luca, N. Bilba, A. Nastro and J. B. Nagy, *Microporous Mesoporous Mater.*, 56 (2002) 227.
- 15 J. B. Nagy, Ph. Bodart, H. Collette, Ch. Fernandez, Z. Gabelica, A. Nastro and R. Aiello, *J. Chem. Soc., Faraday Trans. 1*, 85 (1989) 2749.